

Nonadiabatic Vibrational Resonance Raman Spectra from Quantum Dynamics Propagations with LVC Models. Application to Thymine

Published as part of *The Journal of Physical Chemistry virtual special issue "Vincenzo Barone Festschrift"*.

Qiushuang Xu, Daniel Aranda, Martha Yaghoubi Jouybari, Yanli Liu, Meishan Wang, Javier Cerezo, Roberto Improta, and Fabrizio Santoro*



Cite This: *J. Phys. Chem. A* 2022, 126, 7468–7479



Read Online

ACCESS |



Metrics & More

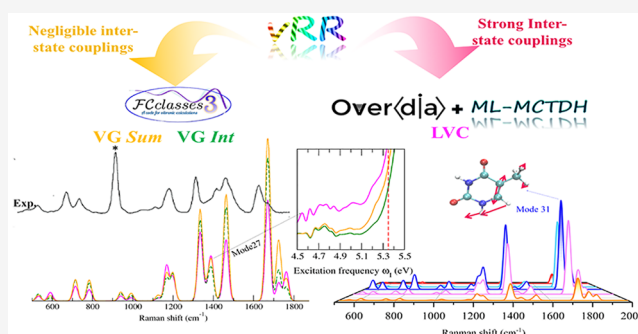


Article Recommendations



Supporting Information

ABSTRACT: We present a viable protocol to compute vibrational resonance Raman (vRR) spectra for systems with several closely lying and potentially coupled electronic states. It is based on the parametrization of linear vibronic coupling (LVC) models from time-dependent density functional theory (TD-DFT) calculations and quantum dynamics propagations of vibronic wavepackets with the multilayer version of the multiconfiguration time-dependent Hartree (ML-MCTDH) method. Our approach is applied to thymine considering seven coupled electronic states, comprising the three lowest bright states, and all vibrational coordinates. Computed vRR at different excitation wavelengths are in good agreement with the available experimental data. Up to 250 nm the signal is dominated by the lowest HOMO \rightarrow LUMO transition, whereas at 233 nm, in the valley between the two lowest energy absorption bands, the contributions of all the three bright states, and their interferences and couplings, are important. Inclusion of solvent (water) effects improves the agreement with experiment, reproducing the coalescence of vibrational bands due to CC and C=O stretchings. With our approach we disentangle and assess the effect of interferences between the contribution of different quasi-resonant states to the transition polarizability and the effect of interstate couplings. Our findings strongly suggest that in cases of close-lying and potentially coupled states a simple inclusion of interference effects is not sufficient, and a fully nonadiabatic computation should instead be performed. We also document that for systems with strong couplings and quasi-degenerate states, the use of HT perturbative approach, not designed for these cases, may lead to large artifacts.



INTRODUCTION

Vibrational resonance Raman (vRR)^{1–3} is a powerful spectroscopic technique to study the properties of molecular excited states. When the excitation energy is close to resonance with the transition energy between the ground state (GS) and an excited state (ES), the contribution of such state to the vibrational transition polarizability is strongly enhanced and possibly dominates all the other ones. In these situations, for a bright resonant ES, the intensity of the vRR band of a specific mode is ruled by the Franck–Condon (FC) integrals between GS and ES vibrational states. This means that such intensity depends primarily on the displacement of the initial and final state equilibrium geometries along such a mode, but it can also be affected by quadratic-terms differences like frequency changes and Duschinsky mixings.

Different effective time-independent (TI)^{4–8} and time-dependent (TD)^{9–12} methods have been proposed to compute vRR in these situations, considering (i) a single resonant ES (ii) with negligible couplings with other ESs. In the following, we will refer to these approaches as “single-state” ones.

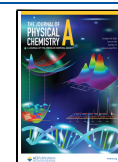
In many molecules, the ES manifold is rather dense so that more than one ES can be in quasi-resonance with the excitation wavelength. In these cases, they all contribute to the transition polarizability and interferences can take place. Assuming that the ES states are not coupled, this situation can still be addressed by computing separately the transition polarizability for each resonant ES, and then summing them up before computing the vRR intensities.¹³

On the other side, when the electronic states are quasi-degenerate, even small interstate couplings can alter their photophysical and spectroscopic behavior. It is thus interesting to investigate, and indeed, it is one of the goals of this study,

Received: July 26, 2022

Revised: August 31, 2022

Published: September 13, 2022



how the interplay between interferences and couplings can affect the vRR signal.

To do that, in this contribution we will resort to a fully nonadiabatic approach based on quantum-dynamical (QD) wave packet propagations on coupled potential energy surfaces (PES). We will use the multiconfiguration TD Hartree (MCTDH)^{14,15} method and, in particular, its multilayer extension (ML-MCTDH).^{16–18} Such propagation techniques are extremely efficient for model Hamiltonians where diabatic states have harmonic PES and the couplings are described by low-order Taylor expansions in the normal coordinates. In particular, we will focus on the linear vibronic coupling (LVC) model, which assumes that normal modes and frequencies of all coupled states coincide with the ground-state ones and considers that interstate couplings are linear functions of the normal coordinates.^{19,20} In fact, we have recently worked out an effective and general approach based on a maximum-overlap diabaticization to parametrize LVC models on the grounds of time-dependent density functional theory (TD-DFT) calculations.^{21,22} Here we will show that, by combining such fast parametrization of LVC models with ML-MCTDH propagations, it is nowadays possible to compute the vRR of systems with several coupled excited states and dozens of normal modes.

Here, as a test case we consider a DNA nucleobase: thymine, Thy. All nucleobases are heteroatom ring structures substituted with functional groups, either a carbonyl or an amino group conjugated with the π system. As a result, they all exhibit close-lying bright and dark states with different properties.^{23,24} The latter, together with the existence of easily accessible conical intersections with the GS are responsible for the rich photophysics exhibited by nucleobases,^{23–27} and their ability to effectively dissipate the energy absorbed by UV radiation,^{23,24} which is potentially harmful and may lead to photodamage.^{23,28} Because of these features, nucleobases are expected to be a good playground to test the computational approach we propose, and to investigate the interplay between interference and interstate couplings in determining the vRR spectra. From a complementary point of view, this study will further assess the potentialities of vRR spectroscopy in disentangling the complex photophysical paths operative in nucleobases.^{29–35}

We will thus compute the vRR spectra of Thy, considering all normal coordinates (39) and a large number of possibly interacting states (7). To test the accuracy of the developed strategy, we will also consider the limit case in which interstate couplings are set to zero. In this case, the LVC Hamiltonian collapses on the so-called Vertical Gradient (VG) model.³⁶ For “single-state” approaches and harmonic PESs, the correlation functions necessary for a TD computation of vRR have an analytical expression,^{37–40} and we rederived and implemented them in our freely available code FCclasses3.⁴¹ We will also use FCclasses3 to investigate the effects of Duschinsky mixings and frequency changes with the Vertical and Adiabatic Hessian (VH and AH) models,^{36,42} comparing their predictions with LVC and VG models in which such effects are neglected. These analytical correlation functions can be derived at both the Franck–Condon (FC) and the Herzberg–Teller (HT) level. The HT perturbative theory⁴³ actually allows us to introduce the effects of weak interstate couplings through the linear dependence of the transition dipoles on the nuclear coordinates, and it is currently included in the most-advanced TI⁴⁴ and TD single-state methods for vRR spectroscopy.^{38,40}

By using the new implementation in FCclasses3, we here investigate the differences between the perturbative HT and nonperturbative LVC approaches and show that, as for absorption,^{45,46} the application of the HT approach for close-lying states with remarkable couplings, i.e., beyond the limits it was conceived for, can give rise to large errors for vRR spectroscopy.

Finally, we investigate solvent effects on the vRR spectra by performing some key calculations both in the gas phase and in water solution, described with implicit solvent models.⁴⁷

THEORY

Let us consider a system with a ground state $|g\rangle$ and a set of coupled electronic diabatic states $|d_i\rangle$. We use a LVC Hamiltonian in the dimensionless normal coordinates \mathbf{q} (and associated momenta \mathbf{p}) of the ground state,

$$\mathbf{H} = \sum_i (K + V_{ii}^{\text{dia}}(\mathbf{q}))|d_i\rangle\langle d_i| + \sum_{i,j>i} V_{ij}^{\text{dia}}(\mathbf{q})(|d_i\rangle\langle d_j| + |d_j\rangle\langle d_i|) \quad (1)$$

The kinetic (K) and potential (V) terms are

$$K = \frac{1}{2} \mathbf{p}^T \mathbf{\Omega} \mathbf{p} \quad (2)$$

$$V_{ii}^{\text{dia}}(\mathbf{q}) = E_i^0 + \lambda_{ii}^T \mathbf{q} + \frac{1}{2} \mathbf{q}^T \mathbf{\Omega} \mathbf{q} \quad (3)$$

$$V_{ij}^{\text{dia}}(\mathbf{q}) = \lambda_{ij}^T \mathbf{q} \quad (4)$$

where $\mathbf{\Omega}$ is the diagonal matrix of the vibrational frequencies of state g . E_i^0 is the i th excited-state energy at the g equilibrium geometry, λ_{ii} is the energy gradient of state i and accounts for a shift of the equilibrium position, and λ_{ij} is the gradient of the interstate coupling $V_{ij}^{\text{dia}}(\mathbf{q})$. Therefore, $V_{ii}^{\text{dia}}(\mathbf{q})$, the PES of diabatic state i , is a quadratic function of \mathbf{q} that shares the same normal modes and frequencies of g and the interstate couplings $V_{ij}^{\text{dia}}(\mathbf{q})$ are linear functions of \mathbf{q} .

Let us consider the following (spectral) representation for the electric dipole moment

$$\hat{\boldsymbol{\mu}} = (\hat{\mu}_x, \hat{\mu}_y, \hat{\mu}_z) = \sum_k \boldsymbol{\mu}^{gk} (|g\rangle\langle d_k| + |d_k\rangle\langle g|) \quad (5)$$

Because we are using a basis set of diabatic states, ideally independent of the coordinates, the vectors $\boldsymbol{\mu}^{gk}$ can be considered constant (FC approximation). The key quantity to compute the vRR spectra from the ground vibrational state ν_0 to the final vibrational state ν_β both associated with the electronic state g , is the transition polarizability tensor

$$\alpha_{\rho\sigma}^{f0}(\omega_1) = \sum_{kn} \frac{\langle g; \nu_f | \hat{\mu}_\rho | d_k; \nu_{kn} \rangle \langle d_k; \nu_{kn} | \hat{\mu}_\sigma | g; \nu_0 \rangle}{E_{kn} - E_{g0} - \hbar\omega_1 - i\hbar\gamma_k} \quad (6)$$

where ρ and σ indicate the Cartesian components, ω_1 is the excitation frequency, E_{g0} is the energy of the initial state, and the sum is over all the possible (quasi-)resonant vibronic states $|d_k; \nu_{kn}\rangle$ with energy E_{kn} and lifetime γ_k . From now on, such a lifetime will be considered independent of k (γ). We now use the following equivalence

$$\lim_{\gamma \rightarrow 0^+} \frac{1}{x - i\hbar\gamma} = \frac{i}{\hbar} \int_0^\infty e^{-i(x-i\hbar\gamma)t/\hbar} dt \quad (7)$$

to obtain

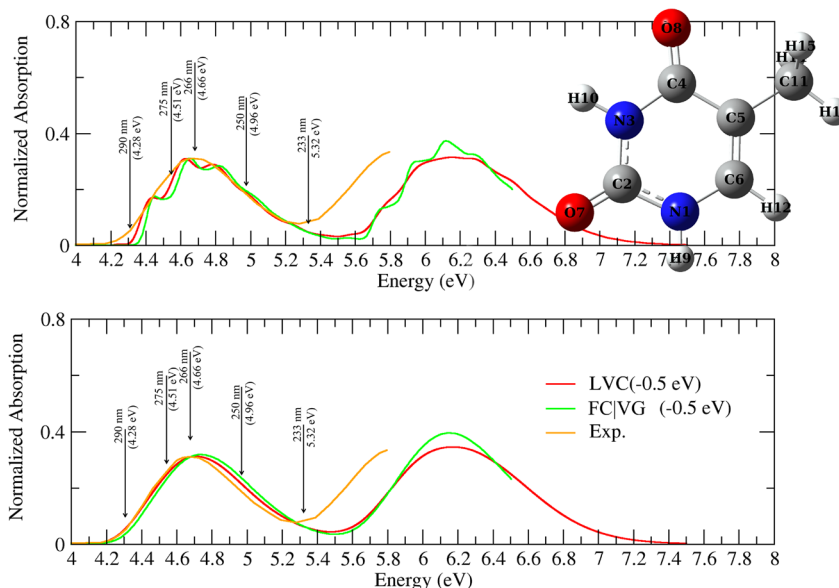


Figure 1. Absorption spectra of thymine computed by FC|VG or LVC models, convoluted with a Gaussian of HWHM = 0.04 eV (top) or 0.12 eV (bottom). Experimental data, in water, from ref 29. Arrows indicate the excitation wavelength used in the vRR experiments in ref 29.

$$\frac{1}{E_{kn} - E_{g0} - \hbar\omega_1 - i\hbar\gamma}$$

$$= \frac{i}{\hbar} \int_0^\infty e^{+i(E_{g0} - E_{kn})t/\hbar + i(\omega_1 + i\gamma)t} dt \quad (8)$$

and therefore, a TD expression of the polarizability tensor

$$\alpha_{\rho\sigma}^{f0}(\omega_1) = \frac{i}{\hbar} \int_0^\infty dt e^{iE_{g0}t/\hbar + i(\omega_1 - \gamma)t}$$

$$\times \sum_{kn} \langle g; v_f | \hat{\mu}_\rho e^{-iE_{kn}/\hbar t} | d_k; v_{kn} \rangle \langle d_k; v_{kn} | \hat{\mu}_\sigma | g; v_0 \rangle \quad (9)$$

Exploiting the fact that $\sum_{kn} |d_k; v_{kn}\rangle \langle d_k; v_{kn}| = 1$ we get

$$\alpha_{\rho\sigma}^{f0}(\omega_1) = \frac{i}{\hbar} \int_0^\infty dt e^{i(E_{g0}/\hbar + \omega_1)t - \gamma t} \langle g; v_f | \hat{\mu}_\rho e^{-i\hbar t/\hbar} \hat{\mu}_\sigma | g; v_0 \rangle \quad (10)$$

Once the transition polarizability is obtained, the vRR intensity can be computed as follows:^{2,44}

$$I(\pi/2, \perp^s + \parallel^s, \perp^\perp) = \frac{\omega_s^4 \mathcal{I}}{16\epsilon_0^2 c_0^4 \pi^2} \frac{45a^2 + 7g^2 + 5d^2}{45} \quad (11)$$

where the rotational invariants a , g^2 , and d^2 are

$$a = \frac{\alpha_{xx}^{f0} + \alpha_{yy}^{f0} + \alpha_{zz}^{f0}}{3}$$

$$g^2 = \frac{1}{2} \left[|\alpha_{xx}^{f0} - \alpha_{yy}^{f0}|^2 + |\alpha_{xx}^{f0} - \alpha_{zz}^{f0}|^2 + |\alpha_{yy}^{f0} - \alpha_{zz}^{f0}|^2 \right. \\ \left. + \frac{3}{2} (|\alpha_{xy}^{f0} + \alpha_{yx}^{f0}|^2 + |\alpha_{xz}^{f0} + \alpha_{zx}^{f0}|^2 + |\alpha_{yz}^{f0} + \alpha_{zy}^{f0}|^2) \right]$$

$$d^2 = \frac{3}{4} (|\alpha_{xy}^{f0} - \alpha_{yx}^{f0}|^2 + |\alpha_{xz}^{f0} - \alpha_{zx}^{f0}|^2 + |\alpha_{yz}^{f0} - \alpha_{zy}^{f0}|^2)$$

In the next section, we describe more in detail the practical protocol we follow to compute the vRR spectra.

Computational Protocol. Let us introduce a more explicit notation for the vibrational states $|v_f\rangle = |0 + 1_f\rangle$, where we clarify that it is a state with 1 quantum on mode f and 0 quanta on all other modes. The ground vibrational state is $|v_0\rangle = |0\rangle$. The vRR spectrum can be computed according to the following steps

- (1) For each bright state $|d_m\rangle$, we start a propagation of a wavepacket obtained vertically exciting the ground vibrational state of the ground state: i.e., $|\Psi(0)\rangle = |d_m; \mathbf{0}\rangle$.
- (2) For each bright diabatic state $|d_k\rangle$ and each vibrational final state $|v_f\rangle = |0 + 1_f\rangle$, we compute the cross-correlation with the bra state $\langle d_k; \mathbf{0} + 1_f|$,

$$\varphi_{km}^{f0}(t) = \langle d_k; \mathbf{0} + 1_f | e^{-iHt/\hbar} | d_m; \mathbf{0} \rangle \quad (13)$$

- (3) We compose the 3×3 tensor of the total correlation function

$$\Phi_{\rho\sigma}^{f0}(t) = \sum_{k,m} \mu_\rho^{gk} \mu_\sigma^{gm} \varphi_{km}^{f0}(t) \quad (14)$$

which corresponds to the bracket in eq 10.

- (4) We perform the Fourier transform for each (ρ, σ) component

$$\alpha_{\rho\sigma}^{f0}(\omega_1) = \frac{i}{\hbar} \int_0^\infty dt e^{iE_{g0}t/\hbar + i\omega_1 t - \gamma t} \Phi_{\rho\sigma}^{f0}(t) \quad (15)$$

where we introduced the Lorentzian damping with width γ .

- (5) We compute the intensity according to eq 11.

It is noteworthy that, in the limiting case in which the resonant diabatic states are uncoupled, for each $|\Psi(0)\rangle = |d_m; \mathbf{0}\rangle$ the only nonvanishing contributions to the total correlation in eq 14 are for $k = m$. Still, $\Phi_{\rho\sigma}^{f0}(t)$ and, therefore, the polarizability tensor α^{f0} is the sum of the contributions of the different resonant states m . This means that interferences effects can arise when squares are taken to compute the rotational invariants. The effect of these interferences was

analyzed in detail for pyrene by some of us in ref 36. To assess the relevance of these interferential effects, here we defined an additional protocol in which the computation of the vRR intensity is simply repeated by considering just one state per time, and then the resulting values are summed (*Sum*).

It is worthy to notice that for vanishing interstate couplings the LVC model collapses into the VG one.³⁶

To summarize this section, when considering more than one quasi-resonant electronic state, we shall compute the vRR intensities by using three different protocols:

- **LVC.** It includes the effects of both interstate couplings and the interference of the different states.
- **VGInt.** It neglects the effects of interstate couplings but considers the interference of the different states, i.e., a sum is taken in eq 14 over all the relevant states k ($k = m$).
- **VGSum.** It neglects the effects of both interstate couplings and interferences. The vRR intensity is thus simply the sum of what is obtained by repeating the computation k times, each of them considering only the ES state k in eq 14. Afterward, the vRR intensities in eq 11 are summed for all relevant states.

As described in detail elsewhere,^{45,48} the absorption (ABS) spectrum can also be formulated as the Fourier transform of (auto)correlation functions, obtained by placing the ground vibrational state at both sides of the bracket in eq 13. The effect of the interstate couplings on the absorption spectra has been here investigated with LVC calculations, which again reduces to VGSum when couplings are neglected.

Computation Details. Electronic calculations were performed with Gaussian16 package of programs,⁴⁹ adopting density functional theory (DFT) level for GS properties and TD-DFT for excited states. The CAM-B3LYP functional in combination with the 6-31G(d) and 6-31G+(d,p) basis set was adopted. The chemical structure of thymine, optimized with C_s symmetry, is shown in Figure 1.

The effect of water solvent was simulated by the PCM (polarizable continuum model) with the linear response implementation,^{47,50} in the nonequilibrium regime for the calculation of the vertical transitions and in the equilibrium one for vibronic ABS and vRR calculations.

After the vRR spectra were computed, for a better comparison with experiments GS vibrational frequencies were scaled by a typical factor 0.96 so to correct for the inaccuracy of the adopted electronic structure theory and for the lack of anharmonic corrections. In the following, if not otherwise specified, we shall report scaled frequencies. QD propagations with ML-MCTDH method were performed with the Quantics code,^{51,52} using a variable mean field (VMF) with a RungeKutta integrator of order 5 and accuracy 10^{-7} for both ABS and vRR spectra. We considered the lowest lying bright states and the close-lying dark states. This choice practically includes the first three $\pi\pi^*$, two $n\pi^*$, and two πRy_n and we adopted TD-DFT to parametrize the corresponding LVC models. For further analysis, spectra were also computed by applying the TD calculation implemented in FCclasses3⁴¹ at 0K based on analytical time-correlation functions. The relevant formulas are reported in the Supporting Information. For these calculations, we adopted VG model, which like LVC neglects the Duschinsky effect and changes of the normal frequencies with the electronic state. To investigate their impact, we also employed VH (the PES of final state is expanded around the

initial equilibrium geometry) and AH (the PES of final state is expanded around its own equilibrium geometry) harmonic models.³⁶

As far as the transition dipole is considered, because electronic states in LVC are diabatic, i.e., because they are ideally independent of the nuclear coordinates, the FC approximation can be invoked in these calculations. For “single state” approaches, though, the considered electronic states are adiabatic and in these cases we considered both the FC and FC+HT approximations.

For ABS, we apply a Gaussian broadening with half-width at half-maximum (HWHM) of 0.04 and 0.12 eV. We compute vRR intensities as 2D functions depending on the incident frequency ω_I and the Raman shift $\omega_I - \omega_S$. The damping constant, γ (see eq 6), was set to either 0.04 or 0.12 eV. The smaller value 0.04 eV was selected because it is very close to the estimated value of the homogeneous contribution to the line width, given in ref 29 (0.044 eV). On the contrary, as shown below, the larger value, 0.12 eV, gives a reasonable reproduction of the experimental absorption shape, thus accounting phenomenologically also for the inhomogeneous broadening. We notice that, formally speaking, homogeneous and inhomogeneous contributions should be added in a two step procedure as done in ref 29. However, results would be similar for what concerns the focus of our paper, and therefore, we avoided this more involved approach. In the conclusions, we comment on possible future developments to include solvent broadening effects in a nonphenomenological way. For better visualization, all the vRR stick spectra have been further convoluted along the Raman shift coordinate with a Gaussian line shape, with HWHM equal to 15 cm^{-1} (when not stated differently).

For a fair comparison between computed and experimental vRR bands, it is necessary to approximately reproduce in the computations the resonance conditions investigated in the experiment. To do that, we first measure the shift of the maxima of the calculated and experimental ABS spectra ($\delta E = E_{\text{max}}^{\text{comp}} - E_{\text{max}}^{\text{exp}}$) and then for an experimental vRR at the excitation frequency ω_I^{exp} , we obtain the excitation to be adopted in the computations ω_I^{comp} with the following formula: $\omega_I^{\text{comp}} = \omega_I^{\text{exp}} + \delta E$.

Further tests reported in the Supporting Information show that, when we switch off the interstate couplings, the spectra obtained with a numerical propagation with ML-MCTDH are virtually indistinguishable from those computed with analytical correlation functions by FCclasses3.⁴¹ For this reason, in the following, we shall label simply as “VG” the spectra obtained with LVC setting to zero the couplings.

RESULTS

Table 1 reports the lowest energy excited states in the gas phase at the FC point, according to CAM-B3LYP/6-31G+(d,p) calculations. The first excited state is a dark $n\pi^*$ state followed by a bright HOMO \rightarrow LUMO bright state, $\pi\pi_1^*$. At significantly higher energies, we find a second $n\pi^*$ state (S_4) and two close-lying bright states, $\pi\pi_2^*$ (S_5) and $\pi\pi_3^*$ (S_6). S_3 and S_7 have a Rydberg character. The situation is similar to the smaller basis set 6-31G(d) (see Table S1 in the Supporting Information), except for a ~ 0.2 eV destabilization of the $\pi\pi^*$ states and for a much larger one of Rydberg states. Confirming previous findings,^{23,26,27,53} as reported in Table S2, inclusion of bulk solvent effects (water) with PCM⁵⁴ leads to a small red

Table 1. Symmetry, Vertical Excitation Energies E_{gf} (eV), Oscillator Strengths (δ_{OPA}) of the First Seven Excited States for Thymine, Calculated with CAM-B3LYP and the 6-311G+(d,p) Basis Sets in the Gas Phase

state	sym	6-311G+(d,p)				
		E_{gf} (eV)	δ_{OPA}	trans	char	coeff
S ₁	A'	5.14	0.00	H-1 → L	$n_O\pi_1^*$	0.63
S ₂	A'	5.31	0.19	H → L	$\pi\pi_1^*$	0.69
S ₃	A''	5.94	0.0006	H → L+1	πRy_{σ_1}	0.69
S ₄	A''	6.47	0.00	H-1 → L+4	$n_O\pi_2^*$	0.40
				H-3 → L+4		
S ₅	A'	6.67	0.055	H-2 → L	$\pi\pi_2^*$	0.69
S ₆	A'	6.73	0.22	H → L+4	$\pi\pi_3^*$	0.66
S ₇	A''	6.78	0.0013	H → L+3	πRy_{σ_2}	0.60

shift of $\pi\pi_1^*$ and to a larger blue shift of $n_O\pi_1^*$, which, as a consequence, invert their relative stability in the FC point.

Absorption Spectra. The vibronic absorption spectra (adopting both LVC and VG models) computed in the gas phase are compared with the experimental spectrum in water²⁹ in Figure 1. The computed spectra are blue-shifted by ~ 0.5 with respect to the experimental ones (first band), and the absorption intensity in the valley at 5.2–5.4 eV is underestimated, mainly because of an overestimation (~ 0.3 eV) of the energy gap between the two lowest energy absorption bands (associated with $\pi\pi_2^*$ and $\pi\pi_3^*$). These discrepancies are partially because of solvent effects. As discussed in detail in the Supporting Information, inclusion of bulk solvent effects red-shifts the computed spectra by 0.1–0.2 eV and decreases the energy gap between the two lowest energy bands by ~ 0.1 eV.

The lack of Duschinsky rotation and frequency changes is another source of error. These effects can be accounted for with AH or VH calculations (neglecting interstate couplings) leading to a red shift of the $\pi\pi_1^*$ band of ~ 0.1 eV (Figure S8 in the Supporting Information). Computations with VH and AH are not feasible for higher lying states because, as a result of

interstate couplings, they feature too many modes with imaginary frequencies. The remaining difference between experiments and calculations is because of inaccuracies of the electronic calculations. In any case, considering the scope of the present study and that a meaningful comparison can only be performed by reproducing resonance conditions similar to those in the experiment (shown as arrows in Figure 1), the vRR spectra have been computed at excitation frequencies blue-shifted by 0.5 eV. Moreover, when discussing the spectra for an excitation at 233 nm (in the valley), we performed test calculations by applying an additional red shift to $\pi\pi_2^*$ and $\pi\pi_3^*$ (see below).

Nonadiabatic effects can be analyzed by comparing the results of the LVC and FCIVG models, and they are only moderate at high resolution (HWHM = 0.04 eV) and almost completely washed out at low resolution (HWHM = 0.12 eV). Interestingly, such large broadening leads to a band shape that agrees with the experimental one.

Vibrational Resonance Raman Spectra. In our approach we compute the nonadiabatic LVC vRR spectrum as a 2D signal, in terms of the excitation frequency ω_1 and the Raman shift (see an example in Figure S1 in the Supporting Information). Typical 1D vRR spectra are then obtained as a section of the 2D signal at a given value of ω_1 . Raman excitation profiles, on the contrary, are 1D cuts for a specific Raman shift, and therefore, they are functions of ω_1 . As mentioned above, calculations were performed with a damping constant, γ , of 0.04 and 0.12 eV. Note that this results in a Lorentzian broadening with HWHM = γ along ω_1 . In both cases, similar vRR spectra are obtained, whereas the Raman excitation profiles are of course smoother (see Figure S6 in the Supporting Information). Although we have shown that a larger broadening provides absorption spectra in better agreement with experiment, in the following, we mainly discuss vRR spectra with $\gamma = 0.04$ eV, because a higher resolution allows us to grasp more easily the differences between the computational models. In Figure 2, we report the

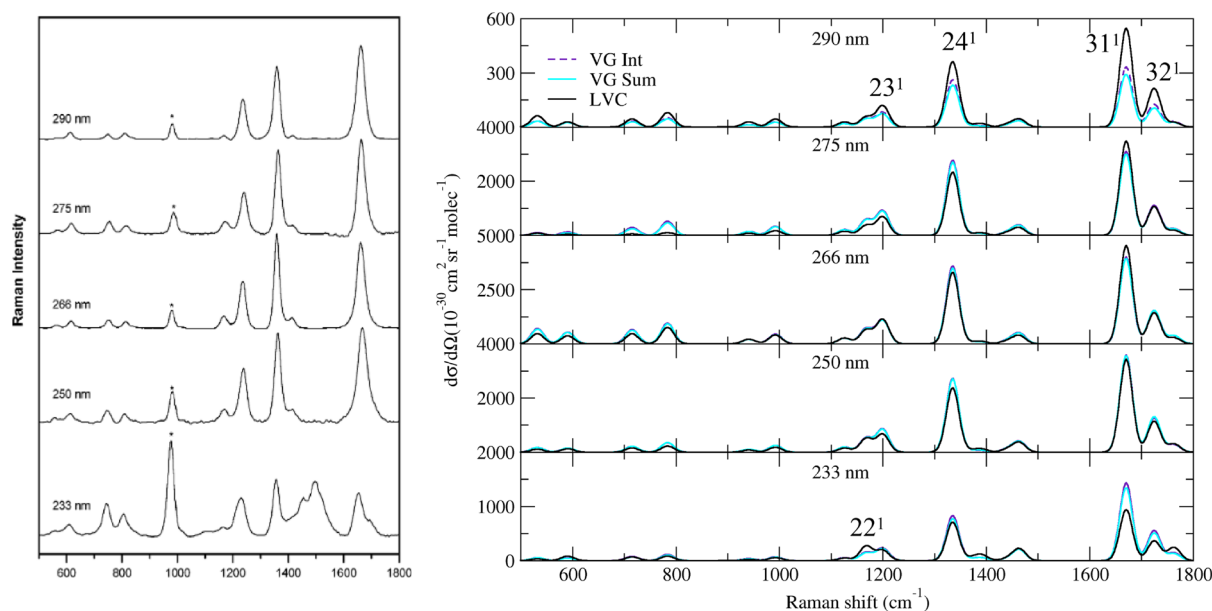


Figure 2. Right panel: Computed vibrational resonance Raman spectra of thymine convoluted with a Lorentzian with damping $\gamma = 0.04$ eV. In the left panel, we report the experimental data in aqueous solutions. Reprinted with permission from ref 29. Copyright 2007 American Chemical Society. The experimental band marked with an asterisk is attributed to the internal standard.

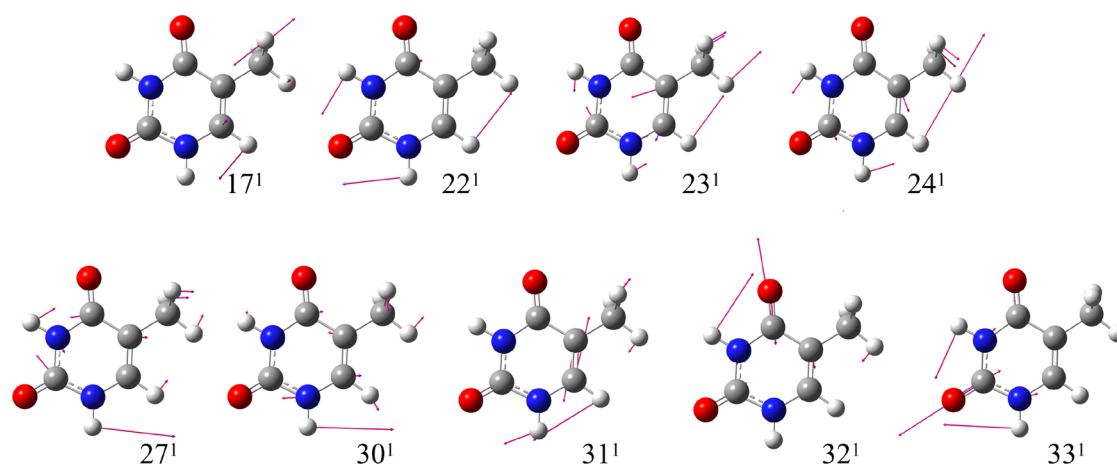


Figure 3. Schematic representation of the most relevant vRR-active vibrational modes of thymine.

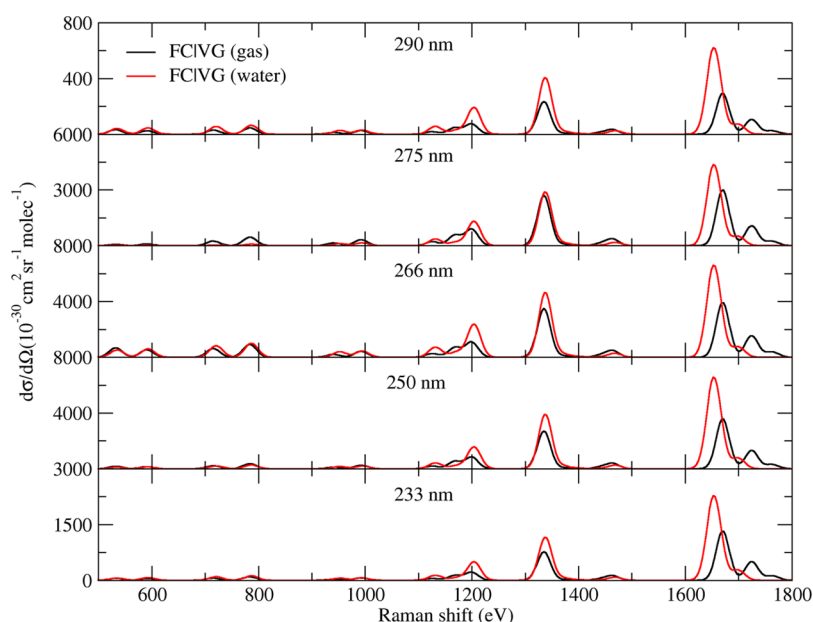


Figure 4. Vibrational resonance Raman spectra of thymine computed by single-state FCIVG model in vacuo and in water, considering only the contribution of $\pi\pi^*$, with a damping $\gamma = 0.04$ eV.

computed and the experimental vRR spectra at excitation wavelengths $\lambda = 290, 273, 266, 250,$ and 233 nm. Our calculations nicely reproduce the experimental line shapes, which are quite similar up to 250 nm. The most intense bands are at 1200, 1335, 1671, and 1725 cm^{-1} . They can be assigned to the fundamentals of modes $23^1, 24^1, 31^1,$ and 32^1 sketched in Figure 3 and corresponding to NH and CH bending, a CC stretching, and a CO stretching.

For excitation frequencies up to 250 nm, it is sufficient to consider the resonance with only the three lowest energy excited states. Figure S7 shows indeed that the LVC results obtained with 7 or 3 states are equivalent. Moreover, nonadiabatic and interferential effects are quite small, as indicated by the close similarity of the results obtained with the three protocols LVC, FCIVGInt, and FCIVGSum (Figure 2). The vRR profile is thus dominated by $\pi\pi^*$, enabling us to focus on this state, with “single state” approaches, for a more in-depth analysis of our results.

One of the major discrepancies with respect to the experiment is observed above 1700 cm^{-1} , where in the

experimental spectrum only one strong band appears, to be compared with the three features present in the computed one (though the one at 1671 cm^{-1} is, by far, the most intense one). They correspond to the C5C6 (see atom labels on Figure 1) stretching (31^1) and to the C4O8 stretching coupled with the bending C2N3H10 (32^1), whereas the very weak shoulder (33^1) is the C2O7 stretching mixed with C2N3H10 and C2N3H9 bendings. Duschinsky mixings and frequency changes are not responsible for the discrepancies between experimental and computational vRR spectra in this region. In fact, Figures S9–S11 of the Supporting Information show that the vRR spectra provided by VG, VH and AH models are similar, although VH and AH Raman excitation profiles are generally smoother than VG ones (Figure S11).

Inclusion of solvent effects is instead crucial to improve the agreement, in that region, with experimental spectra measured in water. As shown in Figure 4, the single-state vRR spectra of $\pi\pi^*$ computed in water and in the gas phase are very similar, except for the bands >1600 cm^{-1} , where for computations in water only one feature is present in much closer agreement

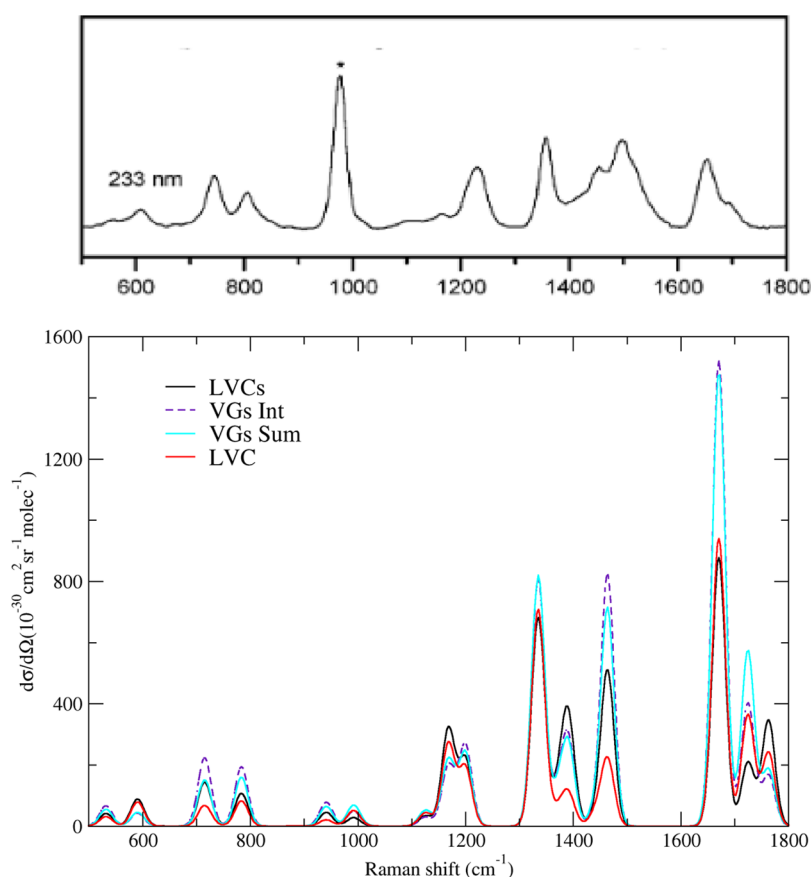


Figure 5. Bottom panel: vibrational resonance Raman spectra computed for thymine, including the lowest energy excited states and red-shifting by 0.3 eV $\pi\pi_2^*$ and $\pi\pi_3^*$ with respect to the other states, at the LVC (LVCs) and at FCIVG level (VCsInt and VGsSum), for an excitation frequency corresponding to 233 nm in the experiment. The LVC vRR spectrum computed without red-shifting $\pi\pi_2^*$ and $\pi\pi_3^*$ is shown for comparison. Top panel: experimental vRR spectrum of thymine in water, following an excitation at 233 nm. Reprinted with permission from ref 29. Copyright 2007 American Chemical Society.

with the experiments. As detailed in Figure S23 of the Supporting Information, in water mode 32 and mode 31 become very close in frequencies (and the relative intensity of the former increases), coalescing in a single band.

In Section S5.3 of the Supporting Information, we investigate the dependence of the results in water on the scaling factor α of the sphere radii adopted to build up the PCM cavity (default $\alpha = 1.1$). The effect is negligible for the shape of the absorption spectrum and small for their position. Concerning the vRR spectra, the effect is small for most of the bands. A partial exception is the band >1600 cm^{-1} discussed above, because the CO stretching is particularly sensitive to the effects. Therefore, for the small value $\alpha = 1.0$, its frequency red-shifts so much to separate from the CC stretching, causing a new splitting of the vRR band which worsens the agreement with experiment. Further details and plots of absorption spectra, vRR spectra at different excitation wavelengths, and Raman excitation profiles for different α values can be found in the Supporting Information.

Closer Look at the vRR Spectrum at 233 nm. We now focus on the vRR spectrum recorded at 233 nm. As shown in Figure 2, at this wavelength a new experimental band at ~ 1500 cm^{-1} appears, which is absent in the computed spectra, both in the gas phase and in water (see Figure 4). Actually, as shown in the Supporting Information, the FCIVG vRR spectra of the higher lying $\pi\pi_2^*$ and $\pi\pi_3^*$ states exhibit two new bands at ~ 1400 and 1450 cm^{-1} , assigned to the fundamentals of modes

27 and 30, which are sketched in Figure S12. However, their intensity is very small, because of the overestimation (by ~ 0.3 eV) of the energy gap between these two states and the lowest energy band.

In Figure 5, we show the LVC vRR spectra computed after artificially red-shifting $\pi\pi_2^*$ and $\pi\pi_3^*$ by ~ 0.3 eV with respect to the three lowest energy excited states (LVCs). Two new intense bands appear at ~ 1450 cm^{-1} (stronger) and ~ 1400 cm^{-1} , in good agreement with the experimental peak at 1500 cm^{-1} and the shoulder at 1450 cm^{-1} . Shifting $\pi\pi_2^*$ and $\pi\pi_3^*$, even the FCIVGsInt model predicts the existence of these two bands (where the “s” label recalls that the shift has been applied). However, the relative intensity of the two bands computed by LVCs is much closer to the experimental one. This finding indicates that the coupling between the three lowest energy bright states modulate the spectroscopic vRR signal. The differences between Int and Sum profiles in Figure 5 clearly highlight that interference has a visible but modest effect, whereas comparison of both results with LVCs ones shows that the impact of interstate couplings is much larger. Further analysis on the relative impact of interstate couplings and interferences is reported in the next section.

Deeper Analysis of Interferential and Nonadiabatic Effects. To analyze more in detail the effect of interstate interferences and couplings, we selected six modes corresponding to the most intense bands 22^1 , 24^1 , 27^1 , 30^1 , 31^1 , and 32^1 , and in Figure 6 we compare their Raman excitation profile

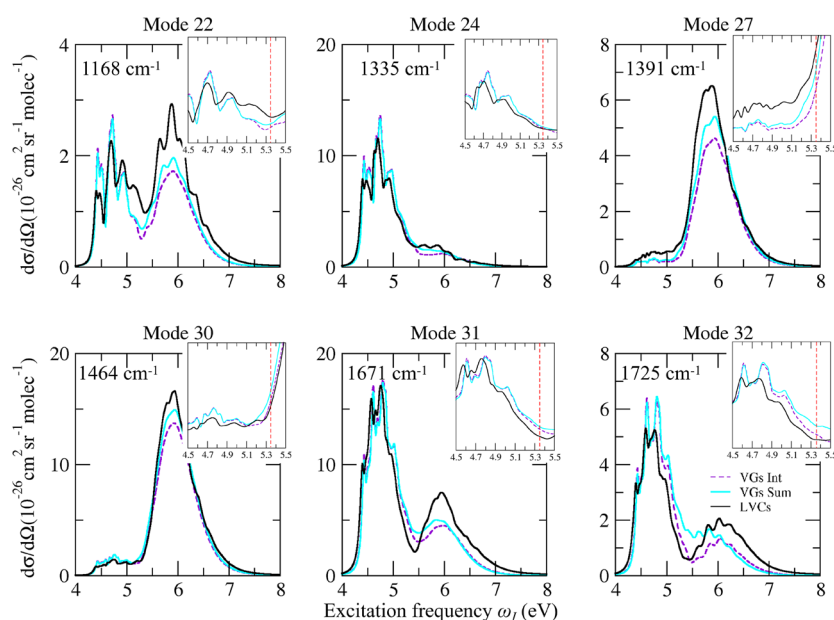


Figure 6. Raman excitation profile of six modes of thymine computed including the seven lowest energy excited states and red-shifting $\pi\pi_2^*$ and $\pi\pi_3^*$ by 0.3 eV with respect to the other states, at the LVC (LVCs, black), FCIVGsInt (purple), and FCIVGsSum (cyan) levels, with a damping $\gamma = 0.04$ eV. The excitation frequencies adopted in the computations to reproduce the experimental resonance conditions are here red-shifted by 0.5 eV. In this way, they match the experimental ones. In particular, the dashed vertical lines in the insets indicate the excitation at 5.32 eV (233 nm).

computed at the nonadiabatic LVC level with those computed by the FCIVGInt and FCIVGsSum models. We consider here the computations in which $\pi\pi_2^*$ and $\pi\pi_3^*$ have been red-shifted by 0.3 eV (the same analysis without the shift is reported in Figure S15 in the Supporting Information). Comparison of FCIVGsSum and FCIVGsInt indicates that interferential effects are present, but they are always modest, except for band 32¹ and $\omega_1 \sim 5.3$ eV. This region corresponds to excitations between the two absorption bands, where the interference is large and destructive (Int intensities are much smaller than Sum ones). As shown by the comparison between LVCs and FCIVGsInt results, the most interesting finding is that nonadiabatic couplings play a much larger role than the interference. In addition to a small loss of the vibronic resolution, nonadiabatic effects change the intensity, mostly in the region at ~ 6.0 eV and at 5.2–5.5 eV. In the former region, corresponding to the second absorption band, the intensity predicted by LVC is always larger. Interestingly, when $\pi\pi_2^*$ and $\pi\pi_3^*$ are not shifted, LVC gives the opposite prediction (see Figure S15 in the Supporting Information), indicating that interstate couplings affect the vRR intensity in a quite complex way. In the valley between the two bands, at 5.2–5.5 eV, LVC is more intense for band 22¹ but less intense for both modes 31¹ and 32¹. Interestingly, only in some cases does FCIVGInt seem to partially capture the difference between LVC and FCIVGsSum, indicating that such a difference is because of interferential effects (check, for example, the Raman profile of band 32¹ at ~ 5.5 eV). In several other cases, FCIVGInt predictions are not even intermediate between FCIVG Sum and LVC (check, for instance, the band 27¹ at ~ 6.0 eV). Because LVC is the “correct” result, we have to conclude that in these cases FCIVGInt is changing FCIVG Sum in the wrong direction. These findings highlight that, for close-lying and potentially coupled states, one should not rely on the simple Int regime and perform calculations like LVC where the effect of couplings is fully taken into account. This conclusion is confirmed by the spectra obtained including only the three bright states in the

LVC model (see Figure S14), which are also different with respect to VGInt predictions.

Contribution of Dark Electronic States. Interstate couplings are expected to strongly enhance the contribution of the dark states. In a perturbative HT treatment, this is easily shown by comparing FCIVG and FCHT/IVG predictions for the $n_0\pi^*$ and $\pi R\gamma_\sigma$. Figure S19 in the Supporting Information documents that, at the FCHT level, new bands appear and other bands increase their intensity by $\sim 10^3$ or even 10^6 . However, at least for A' modes, these bands remain so much weaker than those resulting from the bright states that, in practice, the contribution of dark states cannot be observed. The situation is quite different for the weak signals associated with A'' modes. In fact, their fundamentals are Raman-active only thanks to the nonadiabatic couplings, and according to symmetry, they arise only from the contribution of weak A'' states. It is interesting to notice that, considering different possible protocols within the perturbative approach, this prediction is respected only if we adopt the FCHT approximation only for the weak states and rely on a FC approach for the bright ones. Vice versa, Figure S19 in the Supporting Information documents a dramatic failure of the FCHT approach if it is used also for the bright state $\pi\pi_1^*$. In fact, this protocol predicts a nonphysical and dramatic increase of the Raman signal, which is not observed if we properly apply a nonperturbative method like LVC. Such artifacts have already been described in the calculation of absorption spectra.^{45,46} In Figure 7, we consider the fundamental of one of the A'' modes with the largest HT effect, mode 17 (sketched in Figure 3), and we compare its Raman excitation profile as predicted by LVC, VGInt, and VGSum. We focus on excitations in the first absorption band and include only the contributions of the three lowest energy excited states. VGInt and VGSum results are practically identical, and therefore, interferential effects are negligible. Their intensity correctly reproduces the order of magnitude of the LVC predictions. However, the spectral shapes provided by LVC and VG

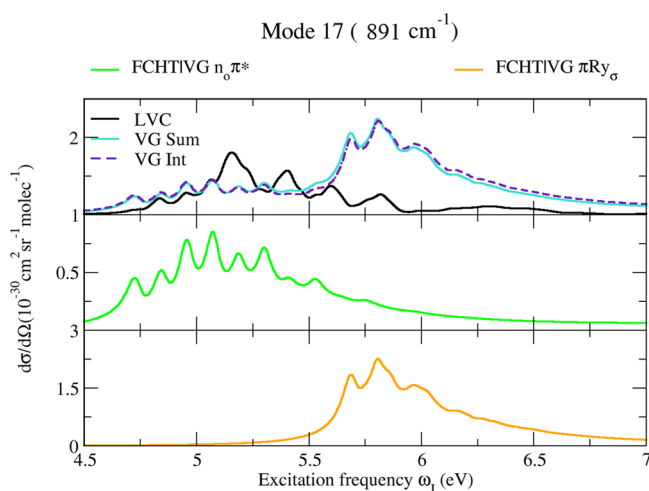


Figure 7. Raman excitation profile of A'' mode 17 of thymine, computed by the LVC model or different possible combinations of FCIVG and FCHTIVG models, considering the three lowest energy excited states and applying a damping $\gamma = 0.04$ eV.

models are quite different. The HT approach overemphasizes the contribution of $n_0\pi^*$ below ~ 4.75 eV and of πRy_σ above ~ 5.5 eV, whereas it underestimates the contribution of $n_0\pi^*$ in the range 4.75 eV $< \omega_1 < 5.5$ eV. Moreover, looking at the vibronic structure, it is possible to trace a one-to-one correspondence for most of the VG and LVC peaks but not for all of them (check, for example, at ~ 5.2 eV). This finding shows that, when states are very close in energy, HT perturbative predictions should be treated with caution. In any case, the predicted intensity of these A'' modes is much weaker than that of the A' ones, and therefore, their experimental detection is very unlikely.

CONCLUDING REMARKS

In this contribution, we presented a viable route to compute vRR spectra for semirigid systems with several close-lying and potentially coupled electronic states. It is based on LVC models and effective ML-MCTDH propagations. The LVC model is parametrized with respect to TD-DFT calculations with a quite general diabaticization technique based on a maximum-overlap criterium that we implemented recently²¹ and interfaced with Gaussian 16.⁵⁵

Our QD approach is similar to that presented by Stock and co-workers years ago⁵⁶ and applied to pyrazine, within a reduced model including two electronic states and seven normal modes. We here show that, by exploiting the recent availability of the very effective ML-MCTDH propagations and the fast LVC parametrization with our approach,^{21,55} it is possible to treat a system like thymine considering all vibrations and a large number (here 7) of coupled states.

Moreover, to get additional insights on the different effects modulating the vRR signal, here we complement the LVC analysis with computations based on analytical expressions of the time-correlation functions, for the limiting cases in which interstate couplings become vanishingly weak. We also compare the predictions of the nonperturbative LVC calculations with those of perturbative HT approaches. Concerning the effects of the coexistence of several quasi-degenerate states for thymine, we investigate to what extent they operate through simple interference or to the fact that the states are actually coupled. Finally, we also get some insights

on the role of environmental effects, by comparing the vRR signals computed in the gas phase and in solution.

We have applied our method to thymine, a prototypical heteroatomic ring, whose photophysical behavior is the focus of ongoing experimental and computational studies.^{23,24,57–60}

The vRR spectra computed in the gas phase are in good agreement with the experimental ones, measured in water, for what concerns both the position and the relative intensity of the different peaks. The only significant discrepancy between the two sets of data concerns the high energy region (>1600 cm^{-1}), where three peaks are present in the computed spectra, to be compared with the single experimental peak. This discrepancy can be corrected by including the solvent effect on the vibrational frequencies, which decreases the stretching frequencies of the CO bonds, leading to their coalescence with that of the CC double bond.

Our study shows that nonadiabatic effects are small for excitation frequencies in resonance with the first electronic band, which is dominated by the lowest bright transition $\pi\pi_1^*$. For this band, frequency changes and Duschinsky mixings are also predicted to play a minor role, thus supporting the reliability of approaches (equivalent to VG) already adopted in the literature in ref 29.

To satisfactorily reproduce the experimental spectrum at 233 nm, corresponding to the valley between the first and second ABS band (due to the contribution of $\pi\pi_2^*$ and, mostly, $\pi\pi_3^*$), it was instead necessary to take into account the contributions of the three lowest bright states ($\pi\pi_1^*$, $\pi\pi_2^*$, and $\pi\pi_3^*$). For vRR in this frequency region, we clearly document remarkable nonadiabatic effects, which are much larger than those from simple interferences. Actually, we show cases in which accounting only for the interference can even change the theoretical predictions in the wrong direction. On this ground, for cases with close-lying states, we can strongly recommend performing a fully nonadiabatic computation.

Nonadiabatic effects play a much larger role on A'' modes, making them Raman active. However, their intensity is predicted to be too small to be detected. It is also noteworthy that we show that improper usage of HT perturbative approach may lead to large artifacts.

Our study provides useful information on the potentialities of vRR for thymine and, more generally, for nucleobases, already a very active research field.^{29–35} Just to make an example, very recently Borrego-Varillas et al.,⁵⁸ documented the involvement of a ring breathing mode at ~ 750 cm^{-1} in the photoexcited dynamics, by adopting a pump–probe set up with sub-30 fs resolution. It is noteworthy that this same mode is actually also seen in the experimental vRR spectra (check Figure 2) and is reproduced by our calculations (it is mode 17 with a frequency of 891 cm^{-1}). Both experimental and computed vRR spectra suggest, moreover, that its involvement should increase for higher excitation energies (233 nm) where also the higher $\pi\pi^*$ states are involved. Our results also suggest that the coupling between $\pi\pi_1^*$ and $n_0\pi^*$ has a larger impact on the vRR of coupling modes with A'' symmetry. In particular, we analyzed the vRR signal of a mode corresponding to the out-of-plane mode of the H bonded to C6 atom, which couples the two states.⁶¹ However, we predict that its intensity is likely too small to make them visible in steady-state vRR experiments. It is very interesting to notice that, with their sub-30 fs experiments, Borrego-Varillas et al.⁵⁸ observed the involvement of such a mode for uridine (where its frequency is smaller) and not in thymidine in water. In this

context, we recall that the possible involvement of dark $n\pi^*$ states in the photophysics of pyrimidines remains a lively debated issue, although for thymine in water it should be very small or even negligible.^{53,58,62,63}

The measurement of vRR spectra for different excitation wavelengths is another useful tool to disentangle the role played by higher energy transitions. We have shown here that our calculations nicely reproduce how the vRR spectrum changes when $\pi\pi_2^*$ and $\pi\pi_3^*$ come into play. We have also shown that at higher excitation frequencies the intensity of the vRR spectrum is remarkably affected by the couplings between the bright states. In this context, it is worthy to notice that the inclusion of the contribution of the higher electronic states allows us to better reproduce the experimental asymmetry of experimental Raman excitation profiles reported for some bands in ref 29 with respect to the simulations performed in the same article considering only $\pi\pi_1^*$ (check Figure S16). These findings suggest that it should be interesting to combine the information gained by vRR with those coming from time-resolved experiments.

Several developments of the approach presented here can be envisaged in the future. In particular, it would be important to tackle an inclusion of solvent effects with explicit models. In fact, because of its high polarity and its capability to establish hydrogen bonds, the effects of water solvent cannot be properly addressed with implicit models.⁶⁴ Explicit water effects might impact the vRR spectra in several ways: not only changing the displacements along the normal modes and their ground-state frequencies or the relative stability of the excited states but also introducing broadening effects. The last two effects have been included only phenomenologically here and in the past.²⁹ In the future, we will investigate the possibility to run the computation of vRR spectra in explicit solvent models, generalizing to resonance Raman the mixed quantum classical approach for absorption spectra in the condensed phase, which we proposed recently both for single-state⁶⁵ and for non-adiabatic systems.⁶⁶ It should be mentioned that, for vRR in explicit water models of systems with negligible nonadiabatic couplings, remarkable progress has been done recently by Gómez et al.,^{67–69} also accounting for the mutual solute/solvent polarization.

■ ASSOCIATED CONTENT

SI Supporting Information

The Supporting Information is available free of charge at <https://pubs.acs.org/doi/10.1021/acs.jpca.2c05271>.

Derivation of the “single-state” analytical correlation functions for vRR for harmonic systems with negligible interstate couplings (FC and HT terms), absorption spectrum in the gas phase with the small 6-31G(d) basis set, further checks and additional plots of the computed vRR spectra with LVC and “single-state” approaches including also frequency changes and Duschinsky effects, excited states in water with PCM and additional computations of vRR spectra in water, also varying the α size cavity parameter (PDF)

■ AUTHOR INFORMATION

Corresponding Author

Fabrizio Santoro – *Consiglio Nazionale delle Ricerche, Istituto di Chimica dei Composti Organo Metallici (ICCOM-CNR),*

I-56124 Pisa, Italy; orcid.org/0000-0003-4402-2685;
Email: fabrizio.santoro@pi.iccom.cnr.it

Authors

- Qiushuang Xu** – *School of Physics and Optoelectronics Engineering, Ludong University, 264025 Yantai, Shandong, PR China; School of Physics Engineering, Qufu Normal University, 2673100 Qufu, Shandong, PR China; Consiglio Nazionale delle Ricerche, Istituto di Chimica dei Composti Organo Metallici (ICCOM-CNR), I-56124 Pisa, Italy*
- Daniel Aranda** – *Instituto de Ciencia Molecular (ICMol), Universidad de Valencia, 46980 Paterna, Spain; orcid.org/0000-0003-0747-6266*
- Martha Yaghoubi Jouybari** – *Consiglio Nazionale delle Ricerche, Istituto di Chimica dei Composti Organo Metallici (ICCOM-CNR), I-56124 Pisa, Italy*
- Yanli Liu** – *School of Physics and Optoelectronics Engineering, Ludong University, 264025 Yantai, Shandong, PR China*
- Meishan Wang** – *School of Physics and Optoelectronics Engineering, Ludong University, 264025 Yantai, Shandong, PR China; orcid.org/0000-0001-8085-2657*
- Javier Cerezo** – *Departamento de Química, Universidad Autónoma de Madrid, 28049 Madrid, Spain; Consiglio Nazionale delle Ricerche, Istituto di Chimica dei Composti Organo Metallici (ICCOM-CNR), I-56124 Pisa, Italy; orcid.org/0000-0003-4820-4371*
- Roberto Improta** – *Consiglio Nazionale delle Ricerche, Istituto di Biostrutture e Bioimmagini (IBB-CNR), I-80145 Napoli, Italy; DTU Chemistry, Technical University of Denmark, DK-2800 Kongens Lyngby, Denmark; orcid.org/0000-0003-1004-195X*

Complete contact information is available at:
<https://pubs.acs.org/10.1021/acs.jpca.2c05271>

Notes

The authors declare no competing financial interest.

■ ACKNOWLEDGMENTS

Q.X. acknowledges the financial support from the China Scholarship Council (CSC, No.202108370212). D.A. acknowledges Fundación Ramón Areces and Generalitat Valenciana/European Social Fund (APOSTD/2021/025) for fundings and ICCOM-CNR (Pisa)/ICMol (Valencia) for hospitality. Y.L. thanks the National Natural Science Foundation of China (Grant No. 11904149). J.C. thanks Ministerio de Universidades, Plan de Recuperación, Transformación y Resiliencia and UAM for funding the research stay in Pisa with a requalification program (CA2/RSUE/2021-00890). R.I. thanks Otto Mønsted Foundation for supporting his stay at DTU and CNR (progetti@cnr/UCATAG4 and Nutrage) for financial support. F.S. thanks progetti@cnr/UCATAG4 and the bilater programme CNR-Royal Society 2021-2022 for financial support.

■ REFERENCES

- (1) Albrecht, A. C. On the theory of Raman intensities. *J. Chem. Phys.* **1961**, *34*, 1476–1484.
- (2) Long, D. A.; Long, D. *The Raman effect: a unified treatment of the theory of Raman scattering by molecules*; Wiley Chichester, 2002; Vol. 8.
- (3) Myers, A. B. Resonance Raman intensities and charge-transfer reorganization energies. *Chem. Rev.* **1996**, *96*, 911–926.

- (4) Dierksen, M.; Grimme, S. An efficient approach for the calculation of Franck–Condon integrals of large molecules. *J. Chem. Phys.* **2005**, *122*, 244101.
- (5) Hazra, A.; Nooijen, M. Derivation and efficient implementation of a recursion formula to calculate harmonic Franck–Condon factors for polyatomic molecules. *Int. J. Quantum Inf.* **2003**, *95* (4–5), 643–657.
- (6) Santoro, F.; Imbrota, R.; Lami, A.; Bloino, J.; Barone, V. Effective method to compute Franck–Condon integrals for optical spectra of large molecules in solution. *J. Chem. Phys.* **2007**, *126*, 084509.
- (7) Santoro, F.; Lami, A.; Imbrota, R.; Bloino, J.; Barone, V. Effective method for the computation of optical spectra of large molecules at finite temperature including the Duschinsky and Herzberg–Teller effect: The Q_x band of porphyrin as a case study. *J. Chem. Phys.* **2008**, *128*, 224311.
- (8) Jankowiak, H.-C.; Stuber, J.; Berger, R. Vibronic transitions in large molecular systems: Rigorous prescreening conditions for Franck–Condon factors. *J. Chem. Phys.* **2007**, *127*, 234101.
- (9) Tang, J.; Lee, M. T.; Lin, S. H. Effects of the Duschinsky mode-mixing mechanism on temperature dependence of electron transfer processes. *J. Chem. Phys.* **2003**, *119*, 7188–7196.
- (10) Ianculescu, R.; Pollak, E. Photoinduced cooling of polyatomic molecules in an electronically excited state in the presence of Dushinskii rotations. *J. Phys. Chem. A* **2004**, *108*, 7778–7784.
- (11) Tatchen, J.; Pollak, E. Ab initio spectroscopy and photoinduced cooling of the trans-stilbene molecule. *J. Chem. Phys.* **2008**, *128*, 164303.
- (12) Barone, V. *Computational strategies for spectroscopy: from small molecules to nano systems*; John Wiley & Sons, 2011.
- (13) Avila Ferrer, F. J.; Barone, V.; Cappelli, C.; Santoro, F. Duschinsky, Herzberg–Teller, and Multiple Electronic Resonance Interferential Effects in Resonance Raman Spectra and Excitation Profiles. The Case of Pyrene. *J. Chem. Theory Comput.* **2013**, *9*, 3597–3611.
- (14) Beck, M. H.; Jäckle, A.; Worth, G. A.; Meyer, H.-D. The multiconfiguration time-dependent Hartree (MCTDH) method: a highly efficient algorithm for propagating wavepackets. *Phys. Rep.* **2000**, *324*, 1–105.
- (15) Meyer, H.-D.; Gatti, F.; Worth, G. A. *Multidimensional quantum dynamics: MCTDH theory and applications*; John Wiley & Sons, 2009.
- (16) Wang, H.; Thoss, M. Multilayer formulation of the multiconfiguration time-dependent Hartree theory. *J. Chem. Phys.* **2003**, *119*, 1289–1299.
- (17) Manthe, U. Layered discrete variable representations and their application within the multiconfigurational time-dependent Hartree approach. *J. Chem. Phys.* **2009**, *130*, 054109.
- (18) Vendrell, O.; Meyer, H.-D. Multilayer multiconfiguration time-dependent Hartree method: Implementation and applications to a Henon–Heiles Hamiltonian and to pyrazine. *J. Chem. Phys.* **2011**, *134*, 044135.
- (19) Köppel, H.; Domcke, W.; Cederbaum, L. Multimode molecular dynamics beyond the Born–Oppenheimer approximation. *Adv. Chem. Phys.* **1984**, *57*, 59–246.
- (20) Köppel, H.; Domcke, W.; Cederbaum, L. In *Conical intersections: Electronic structure, dynamics and spectroscopy*; Domcke, W., Yarkony, D., Köppel, H., Eds.; World Scientific Publishing Co. Pte. Ltd., Singapore, 2004; Chapter 7, pp 323–367.
- (21) Yaghoubi Jouybari, M.; Liu, Y.; Imbrota, R.; Santoro, F. Ultrafast dynamics of the two lowest bright excited states of cytosine and 1-methylcytosine: A quantum dynamical study. *J. Chem. Theory Comput.* **2020**, *16*, 5792–5808.
- (22) Green, J. A.; Yaghoubi Jouybari, M.; Asha, H.; Santoro, F.; Imbrota, R. Fragment Diabatization Linear Vibronic Coupling Model for Quantum Dynamics of Multichromophoric Systems: Population of the Charge-Transfer State in the Photoexcited Guanine–Cytosine Pair. *J. Chem. Theory Comput.* **2021**, *17*, 4660–4674.
- (23) Imbrota, R.; Santoro, F.; Blancafort, L. Quantum mechanical studies on the photophysics and the photochemistry of nucleic acids and nucleobases. *Chem. Rev.* **2016**, *116*, 3540–3593.
- (24) Barbatti, M.; Borin, C. A.; Ullrich, S. *Photoinduced Phenomena in Nucleic Acids I: Nucleobases in the Gas Phase and in Solvents*; Springer International Publishing: Cham, Switzerland, 2015; Vol. 355, pp 1–358.
- (25) Gustavsson, T.; Imbrota, R.; Markovitsi, D. DNA/RNA: Building Blocks of Life Under UV Irradiation. *J. Phys. Chem. Lett.* **2010**, *1*, 2025–2030.
- (26) Gustavsson, T.; Bányász, Á.; Lazzarotto, E.; Markovitsi, D.; Scalmani, G.; Frisch, M. J.; Barone, V.; Imbrota, R. Singlet Excited-State Behavior of Uracil and Thymine in Aqueous Solution: A Combined Experimental and Computational Study of 11 Uracil Derivatives. *J. Am. Chem. Soc.* **2006**, *128*, 607–619.
- (27) Santoro, F.; Barone, V.; Gustavsson, T.; Imbrota, R. Solvent effect on the singlet excited-state lifetimes of nucleic acid bases: A computational study of 5-fluorouracil and uracil in acetonitrile and water. *J. Am. Chem. Soc.* **2006**, *128*, 16312–22.
- (28) Imbrota, R.; Douki, T. *DNA Photodamage: From Light Absorption to Cellular Responses and Skin Cancer*; Royal Society of Chemistry, 2021.
- (29) Yarasi, S.; Brost, P.; Loppnow, G. R. Initial excited-state structural dynamics of thymine are coincident with the expected photochemical dynamics. *J. Phys. Chem. A* **2007**, *111*, 5130–5135.
- (30) Oladepo, S. A.; Loppnow, G. R. Initial excited-state structural dynamics of 9-methyladenine from uv resonance raman spectroscopy. *J. Phys. Chem. B* **2011**, *115*, 6149–6156.
- (31) Billinghurst, B. E.; Loppnow, G. R. Excited-state structural dynamics of cytosine from resonance Raman spectroscopy. *J. Phys. Chem. A* **2006**, *110*, 2353–2359.
- (32) Yarasi, S.; Ng, S.; Loppnow, G. R. Initial excited-state structural dynamics of uracil from resonance Raman spectroscopy are different from those of thymine (5-methyluracil). *J. Phys. Chem. B* **2009**, *113*, 14336–14342.
- (33) Sasidharanpillai, S.; Loppnow, G. R. Initial Excited-State Structural Dynamics of dT and dA Oligonucleotide Homopentamers Using Resonance Raman Spectroscopy. *J. Phys. Chem. B* **2019**, *123*, 3898–3906.
- (34) Billinghurst, B. E.; Oladepo, S. A.; Loppnow, G. R. Initial Excited-State Structural Dynamics of Thymine Derivatives. *J. Phys. Chem. B* **2012**, *116*, 10496.
- (35) El-Yazbi, A. F.; Palech, A.; Loppnow, G. R. Initial Excited-State Structural Dynamics of 2'-Deoxyguanosine Determined via UV Resonance Raman Spectroscopy. *J. Phys. Chem. A* **2011**, *115*, 10445.
- (36) Avila Ferrer, F. J.; Santoro, F. Comparison of vertical and adiabatic harmonic approaches for the calculation of the vibrational structure of electronic spectra. *Phys. Chem. Chem. Phys.* **2012**, *14*, 13549–13563.
- (37) Tannor, D. J.; Heller, E. J. Polyatomic Raman scattering for general harmonic potentials. *J. Chem. Phys.* **1982**, *77*, 202–218.
- (38) Ma, H.; Liu, J.; Liang, W. Time-Dependent Approach to Resonance Raman Spectra Including Duschinsky Rotation and Herzberg–Teller Effects: Formalism and Its Realistic Applications. *J. Chem. Theory Comput.* **2012**, *8*, 4474–4482.
- (39) Banerjee, S.; Kröner, D.; Saalfrank, P. Resonance Raman and vibronic absorption spectra with Duschinsky rotation from a time-dependent perspective: Application to β -carotene. *J. Chem. Phys.* **2012**, *137*, 22A534.
- (40) Baiardi, A.; Bloino, J.; Barone, V. Accurate Simulation of Resonance-Raman Spectra of Flexible Molecules: An Internal Coordinates Approach. *J. Chem. Theory Comput.* **2015**, *11*, 3267–3280.
- (41) Santoro, F.; Cerezo, J. *FCclasses 3, a code for vibronic calculations*; ICCOM, 2022; <http://www.iccom.cnr.it/en/fcclasses> (accessed on 30 Aug. 2022).
- (42) Cerezo, J.; Santoro, F. Revisiting Vertical Models To Simulate the Line Shape of Electronic Spectra Adopting Cartesian and Internal Coordinates. *J. Chem. Theory Comput.* **2016**, *12*, 4970–4985.
- (43) Herzberg, G.; Teller, E. Schwingungsstruktur der Elektronenübergänge bei mehratomigen Molekülen. *Z. Phys. Chem.* **1933**, *21B*, 410–446.

- (44) Santoro, F.; Cappelli, C.; Barone, V. Effective Time-Independent Calculations of Vibrational Resonance Raman Spectra of Isolated and Solvated Molecules Including Duschinsky and Herzberg–Teller Effects. *J. Chem. Theory Comput.* **2011**, *7*, 1824–1839.
- (45) Aranda, D.; Santoro, F. Vibronic spectra of π -conjugated systems with a multitude of coupled states: A protocol based on linear vibronic coupling models and quantum dynamics tested on hexahelicene. *J. Chem. Theory Comput.* **2021**, *17*, 1691–1700.
- (46) Liu, Y.; Aranda, D.; Santoro, F. A computational study of the vibronic effects on the electronic spectra and the photophysics of aza [7] helicene. *Phys. Chem. Chem. Phys.* **2021**, *23*, 16551–16563.
- (47) Tomasi, J.; Mennucci, B.; Cammi, R. Quantum mechanical continuum solvation models. *Chem. Rev.* **2005**, *105*, 2999–3094.
- (48) Liu, Y.; Martínez-Fernández, L.; Cerezo, J.; Prampolini, G.; Improta, R.; Santoro, F. Multistate coupled quantum dynamics of photoexcited cytosine in gas-phase: Nonadiabatic absorption spectrum and ultrafast internal conversions. *Chem. Phys.* **2018**, *515*, 452–463.
- (49) Frisch, M. J.; et al. *Gaussian 16 Revision B.01*; Gaussian Inc.: Wallingford, CT, 2016.
- (50) Cossi, M.; Barone, V. Time-dependent density functional theory for molecules in liquid solutions. *J. Chem. Phys.* **2001**, *115*, 4708–4717.
- (51) Worth, G. A.; Giri, K.; Richings, G. W.; Beck, M. H.; Jäckle, A.; Meyer, H.-D. *QUANTICS Package*, Version 1.1; University of Birmingham, Birmingham, U.K., 2015.
- (52) Worth, G. Quantics: A general purpose package for Quantum molecular dynamics simulations. *Comput. Phys. Commun.* **2020**, *248*, 107040.
- (53) Cerezo, J.; Liu, Y.; Lin, N.; Zhao, X.; Improta, R.; Santoro, F. Mixed Quantum/Classical Method for Nonadiabatic Quantum Dynamics in Explicit Solvent Models: The $\pi\pi^*/n\pi^*$ Decay of Thymine in Water as a Test Case. *J. Chem. Theory Comput.* **2018**, *14*, 820–832.
- (54) Tomasi, J.; Mennucci, B.; Cammi, R. Quantum mechanical continuum solvation models. *Chem. Rev.* **2005**, *105*, 2999–3094.
- (55) Santoro, F.; Green, J. A. *Overdia 01, a Fortran 90 code for parametrization of model Hamiltonians based on a maximum-overlap diabatisation*; ICCOM, 2022; <http://www.iccom.cnr.it/en/overdia-en> (accessed on 30 Aug 2022).
- (56) Stock, G.; Woywod, C.; Domcke, W.; Swinney, T.; Hudson, B. S. Resonance Raman spectroscopy of the S1 and S2 states of pyrazine: Experiment and first principles calculation of spectra. *J. Chem. Phys.* **1995**, *103*, 6851–6860.
- (57) Erickson, B. A.; Heim, Z. N.; Pieri, E.; Liu, E.; Martinez, T. J.; Neumark, D. M. Relaxation Dynamics of Hydrated Thymine, Thymidine, and Thymidine Monophosphate Probed by Liquid Jet Time-Resolved Photoelectron Spectroscopy. *J. Phys. Chem. A* **2019**, *123*, 10676–10684.
- (58) Borrego-Varillas, R.; Nenov, A.; Kabaciński, P.; Conti, I.; Ganzer, L.; Oriana, A.; Jaiswal, V. K.; Delfino, I.; Weingart, O.; Manzoni, C.; et al. Tracking excited state decay mechanisms of pyrimidine nucleosides in real time. *Nat. Commun.* **2021**, *12*, 7285.
- (59) Fedotov, D. A.; Paul, A. C.; Koch, H.; Santoro, F.; Coriani, S.; Improta, R. Excited state absorption of DNA bases in the gas phase and in chloroform solution: a comparative quantum mechanical study. *Phys. Chem. Chem. Phys.* **2022**, *24*, 4987–5000.
- (60) Martínez Fernández, L.; Santoro, F.; Improta, R. Nucleic Acids as a Playground for the Computational Study of the Photophysics and Photochemistry of Multichromophore Assemblies. *Acc. Chem. Res.* **2022**, *55* (15), 2077–2087.
- (61) Improta, R.; Barone, V.; Lami, A.; Santoro, F. Quantum Dynamics of the Ultrafast $\pi\pi^*/n\pi^*$ Population Transfer in Uracil and 5-Fluoro-Uracil in Water and Acetonitrile. *J. Phys. Chem. B* **2009**, *113*, 14491–14503.
- (62) Hare, P. M.; Crespo-Hernández, C. E.; Kohler, B. Internal conversion to the electronic ground state occurs via two distinct pathways for pyrimidine bases in aqueous solution. *Proc. Natl. Acad. Sci.* **2007**, *104*, 435–440.
- (63) Buchner, F.; Nakayama, A.; Yamazaki, S.; Ritze, H.-H.; Lübcke, A. Excited-State Relaxation of Hydrated Thymine and Thymidine Measured by Liquid-Jet Photoelectron Spectroscopy: Experiment and Simulation. *J. Am. Chem. Soc.* **2015**, *137*, 2931–2938.
- (64) Giovannini, T.; Egidi, F.; Cappelli, C. Molecular spectroscopy of aqueous solutions: a theoretical perspective. *Chem. Soc. Rev.* **2020**, *49*, 5664–5677.
- (65) Cerezo, J.; Aranda, D.; Avila Ferrer, F. J.; Prampolini, G.; Santoro, F. Adiabatic-Molecular Dynamics Generalized Vertical Hessian Approach: A Mixed Quantum Classical Method To Compute Electronic Spectra of Flexible Molecules in the Condensed Phase. *J. Chem. Theory Comput.* **2020**, *16*, 1215–1231.
- (66) Segalina, A.; Aranda, D.; Green, J. A.; Cristino, V.; Caramori, S.; Prampolini, G.; Pastore, M.; Santoro, F. How the Interplay among Conformational Disorder, Solvation, Local, and Charge-Transfer Excitations Affects the Absorption Spectrum and Photoinduced Dynamics of Perylene Diimide Dimers: A Molecular Dynamics/Quantum Vibronic Approach. *J. Chem. Theory Comput.* **2022**, *18*, 3718–3736.
- (67) Gómez, S.; Egidi, F.; Puglisi, A.; Giovannini, T.; Rossi, B.; Cappelli, C. Unlocking the power of resonance Raman spectroscopy: The case of amides in aqueous solution. *J. Mol. Liq.* **2022**, *346*, 117841.
- (68) Gómez, S.; Bottari, C.; Egidi, F.; Giovannini, T.; Rossi, B.; Cappelli, C. Amide Spectral Fingerprints are Hydrogen Bonding-Mediated. *J. Phys. Chem. Lett.* **2022**, *13*, 6200–6207.
- (69) Gómez, S.; Rojas-Valencia, N.; Giovannini, T.; Restrepo, A.; Cappelli, C. Ring Vibrations to Sense Anionic Ibuprofen in Aqueous Solution as Revealed by Resonance Raman. *Molecules* **2022**, *27*, 442.